



# Probabilistic mapping of life loss due to dam-break flooding

Andrea Maranzoni<sup>1</sup> · Marco D'Oria<sup>1</sup> · Carmine Rizzo<sup>1</sup>

Received: 19 July 2023 / Accepted: 19 October 2023 / Published online: 29 November 2023  
© The Author(s) 2023

## Abstract

Assessment of flood damage caused by dam failures is typically performed deterministically on the basis of a single preselected scenario, neglecting uncertainties in dam-break parameters, exposure information, and vulnerability model. This paper proposes a probabilistic flood damage model for the estimation of life loss due to dam-break flooding with the aim of overcoming this limitation and performing a more comprehensive and informative evaluation of flood risk. The significant novelty lies in the fact that the model combines uncertainties associated with all three components of risk: hazard, exposure, and vulnerability. Uncertainty in flood hazard is introduced by considering a set of dam-break scenarios, each characterized by different breach widths and reservoir levels. Each scenario is linked to a probability, which is assumed conditional on the dam-break event. Uncertainty in exposure is accounted for using dasymetric maps of the population at risk for two socio-economic states (representing business and non-business hours of a typical week), along with associated likelihood. Vulnerability to flooding is described through a well-established empirical hazard-loss function relating the fatality rate of the population at risk to the flood hazard, the flood severity understanding, and the warning time; a confidence band provides quantitative information about the associated uncertainty. The probabilistic damage model was applied to the case study of the hypothetical collapse of Mignano concrete gravity dam (northern Italy). The main outcome is represented by probabilistic flood damage maps, which show the spatial distribution of selected percentiles of a loss-of-life risk index coupled with the corresponding uncertainty bounds.

**Keywords** Dam-break · Failure scenarios · Flood damage · Loss of life · Probabilistic maps · Uncertainty

## 1 Introduction

Impounding water in artificial reservoirs formed by dams offers many benefits, such as water supply, irrigation, hydropower generation, and flood control, thereby contributing to economic development and social welfare. However, in the unfortunate event of their failure, dams pose a potentially severe risk to the safety of the population, infrastructures,

---

✉ Andrea Maranzoni  
andrea.maranzoni@unipr.it

<sup>1</sup> Department of Engineering and Architecture, University of Parma, Parma, Italy

economic activities, as well as historical and environmental assets located downstream (Saxena and Sharma 2004). Indeed, the resulting dam-break flooding may involve vast areas, potentially leading to direct and indirect catastrophic consequences, including loss of life (Lumbroso et al. 2011; Ge et al. 2017), as well as substantial economic and societal impacts (Ge et al. 2020). Despite the established, widespread recognition of the importance of dam safety in preventing or, at least, reducing risks associated with dam-related hazards (Rodrigues et al. 2002), many dam failures have occurred worldwide (Zhang et al. 2016; Aureli et al. 2021), some with calamitous consequences, including significant loss of life (Costa 1985; Chanson 2004; Lumbroso et al. 2011; Zhang et al. 2016). Although dam-break events are infrequent (according to Costa 1985, the probability of dam failure is on the order of  $10^{-4}$  per dam-year), there is potential for an increase in the occurrence of dam incidents and accidents in the future, due to dam ageing (Perera et al. 2021) and the impact of climate change on dam safety (Fluixá-Sanmartín et al. 2018).

The consequences of flooding derive from the combination of three factors: flood hazard, flood exposure, and flood vulnerability (Hartford and Baecher 2004; Merz et al. 2007; Cardona et al. 2012; de Moel et al. 2015; Li et al. 2018). Vulnerability analysis relates the predicted local flood hazard magnitude to the ensuing damages for the selected exposed elements. The quantitative assessment and mapping of the flood damage potentially resulting from a hypothetical dam-break are essential to support emergency response planning and preparation, and define mitigation measures (Rodrigues et al. 2002; Qi and Altınakar 2012) to reduce the adverse consequences of flooding (Bates 2022; Silva and Eleutério 2023a).

A comprehensive analysis of dam-break flooding consequences should consider the population at risk within the potentially flooded area, along with societal, economic, and environmental impacts (Sun et al. 2014; Sarchani and Koutroulis 2022). However, since loss of life is the most severe consequence of a catastrophic event such as flooding (Silva and Eleutério 2023b), preventing loss of human lives is the main concern in emergency management following a dam failure. For this reason, this paper focuses on this aspect of the flooding damage.

Two different methodologies are available to estimate flood casualties. The simplest one, which is used in this paper, is based on empirical hazard-loss functions (DeKay and McClelland 1993; Graham 1999; RESCDAM 2001; McClelland and Bowles 2002; Penning-Rowsell et al. 2005; Jonkman and Vrijling 2008; Jonkman et al. 2008), which express the damaging effect of the flooding on the population at risk via a fatality rate. More complex micro-scale agent-based models have recently gained attention, as they provide a physical interpretation of the processes contributing to the determination of life loss, especially the population redistribution during the evacuation (see, for example, LIFESim (Aboelata and Bowles 2005; Bowles and Aboelata 2006); HEC-LifeSim (CEIWR-HEC 2020); Hazus-MH (FEMA 2021); Life Safety Model (Johnstone et al. 2005; Lumbroso et al. 2011); TU Delft method (Asselman and Jonkman 2003); etc.). Reviews and comparisons of state-of-the-art methods for estimating loss of life resulting from catastrophic floods are provided by Johnstone and Lence (2009), Lumbroso et al. (2011), Di Mauro et al. (2012), and Norkhairi et al. (2018), among others.

Emergency Action Plans (EAPs) are non-structural tools globally used to establish operational strategies and coordinated actions for dam-break flood risk management, and to identify the institutional subjects and government agencies committed to ensuring the safety of the population at risk (ASDSO 2023). As an example, the Directive of the Italian Prime Minister of 8 July 2014 on large dams provides operational guidelines for civil protection activities in the event of a dam failure and identifies the responsibility

of all involved parties (dam owners, agencies and authorities) in the emergency management. FEMA (2013) provides guidelines for creating inundation maps for EAPs.

In EAPs, preplanned actions for handling emergencies caused by dam accidents typically rely on a flood exposure map, which combines socio-economic information (i.e. population distribution; location of buildings, economic activities, infrastructures, and strategic services; land use; etc.) with flood hazard information (mainly the expected flooded area) obtained by considering a single (albeit precautionary) dam-break scenario. For instance, in the case of concrete and masonry dams, the Circular from the Italian Prime Minister 13.12.1995, n. DSTN/2/22806 prescribes that the dam-break analysis is performed deterministically by considering the worst-case scenario (not linked to extreme hydrological events) of instantaneous and total collapse of the dam, with the reservoir level at the spillway crest. This scenario coincides with the ‘sunny day’ failure scenario that national agencies responsible for supervising dam design, construction, and management recommend considering for concrete and masonry dams (e.g. FEMA 2013; NZSOLD 2015; CDSO 2018).

The literature offers numerous examples of event-based flood damage assessments focusing on hypothetical or historical dam-breaks (Lumbroso et al. 2011; Yerramilli 2013; El Bilali et al. 2021; de Oliveira et al. 2022), but also on riverine floods with a given return period (e.g. Masood and Takeuci 2012). However, flood damage assessment, especially when related to hypothetical dam failures, is affected by significant uncertainties due to the various relevant factors involved (Apel et al. 2004; de Moel et al. 2015; Wagenaar et al. 2016; Beven et al. 2018). Therefore, it is crucial to include a quantitative analysis of the uncertainty and effectively communicate it to enhance efficient decision-making in flood risk and emergency management (Beven et al. 2015; Poortvliet et al. 2019). In this regard, Wagenaar et al. (2016) state that “a quantification of the uncertainty in the damage estimates can help to get an insight in the potential error that can occur in a decision based on the flood damage estimate and may improve the decision-making process”. A probabilistic approach, already commonly used in hazard and risk assessments for riverine and levee breach flooding (Vorogushyn et al. 2010; D’Oria et al. 2019; Maranzoni et al. 2022), can be advantageous to this purpose (Tsai et al. 2019; El Bilali et al. 2022; Rizzo et al. 2023).

This study focuses on probabilistic dam-break flood damage assessment in terms of loss of life, incorporating uncertainty into damage estimation (Egorova et al. 2008; de Moel and Aerts 2011). It proposes a probabilistic method for estimating dam-break flooding fatalities, which simultaneously includes the uncertainties associated with flood hazard, flood exposure, and the flood vulnerability model. Uncertainty in flood hazard is addressed by considering a set of dam-break scenarios (Paşa et al. 2023; Rizzo et al. 2023) differing in the values of two key input parameters: breach width and reservoir level. Each scenario is assigned a conditional probability, given the occurrence of a dam-break event. Epistemic uncertainty in flood exposure is accounted for by incorporating two different population distributions corresponding to relevant socio-economic states during business and non-business hours, with associated likelihoods of occurrence. Uncertainty in the hazard-damage function (describing the uncertain susceptibility of the population at risk to flooding in terms of fatality rate) is included through loss uncertainty bounds (Graham 1999; Sun et al. 2014). These bounds can be treated as confidence intervals for a given confidence level. To our knowledge, a probabilistic damage model considering the uncertainties in all damage components is an innovative advancement in risk-based dam-break flood management (de Moel et al. 2015). Moreover, a probabilistic approach based on the preselection of dam-break scenarios and socio-economic states with associated probabilities potentially reduces

the computational effort required by probabilistic flood damage models based on Monte Carlo methods (e.g. Egorova et al. 2008).

The reliability and applicability of the proposed method are demonstrated by producing probabilistic damage maps (in terms of loss of life) for the case study of the hypothetical failure of Mignano dam, a concrete gravity dam located in the upper course of the River Arda in northern Italy.

## 2 Method

Figure 1 sketches the concept of the probabilistic flood damage method. All three components of the flood risk (i.e. flood hazard, flood exposure and flood vulnerability) are treated probabilistically. Probabilistic flood hazard assessment (step a) is developed through the following sub-steps: (a1) define a set of representative dam-break scenarios with associated probabilities; (a2) use hydrodynamic modelling to simulate the inundation resulting from each dam-break scenario; and (a3) create flood hazard maps for each dam-break scenario based on a chosen flood hazard classification. Flood exposure assessment (step b) consists in (b1) defining representative socio-economic states with their associated likelihoods; (b2) using demographic data (derived from choropleth maps) and land use maps to (b3) establish dasymmetric population density maps downstream of the dam for each socio-economic scenario; and (b4) overlaying the flood hazard and population density maps to generate flood exposure maps (which identify the population at risk) along with the associated compound probabilities. Flood vulnerability assessment relies on a suitable empirical flood hazard-fatality rate function (step c). Finally, flood damage evaluation (step d) includes

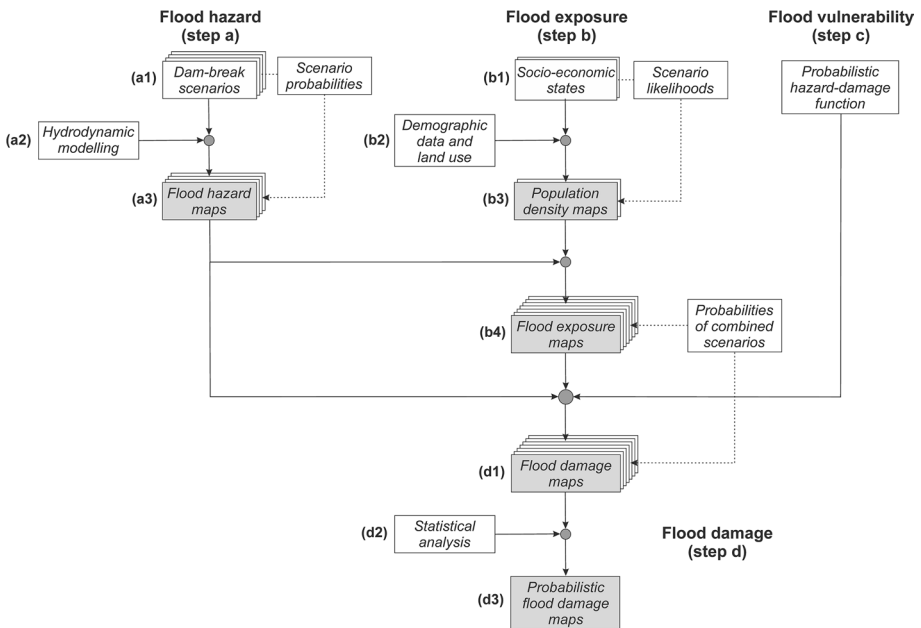


Fig. 1 Conceptual sketch of the probabilistic method for dam-break flood damage assessment

(d1) calculating flood damage maps of life loss for each combination of dam-break scenarios and socio-economic conditions, along with associated compound probabilities, and (d2) conducting a statistical analysis on the ensemble of flood damage maps based on the corresponding compound probabilities to (d3) obtain probabilistic flood damage maps providing the spatial distribution of a suitable flood risk index (expressed in terms of loss of life) together with information about the associated uncertainty.

The methodology was implemented through geographic information system (GIS) and MATLAB environments. We conducted the initial basic operations on the raster data in GIS, while we carried out complex calculations and statistical analyses in MATLAB, treating the raster data as matrices. The MATLAB results were then converted back into raster format and visualized within the GIS platform. This mode of operation allowed us to efficiently overcome the problem posed by the gap between mathematical computations and GIS-based visualization.

## 2.1 Flood hazard

The flood hazard assessment step is based on a set of dam-break scenarios differing in reservoir level and breach width, thereby accounting for uncertainties in the initial hydrologic conditions and the breach size (Rizzo et al. 2023). The breach formation time can be excluded from the uncertain variables in risk analyses concerning concrete or masonry dam failures since such dams tend to fail abruptly (e.g. NZSOLD 2015; CDSO 2018). In the ‘sunny day’ failure scenario, the inflow to the reservoir can also be neglected, and the downstream river reach can be assumed initially dry since dam-break flow conditions are expected to be much more severe than normal ones (e.g. Pilotti et al. 2011; Ferrari et al. 2023).

The ranges of variability for the two parameters considered (reservoir level and breach width) are discretized into distinct classes, which are then combined to define the dam-break scenarios. Each scenario is assigned a probability, which is assumed to be conditional on the occurrence of a dam-break event, according to the method suggested by Rizzo et al. (2023). Accordingly, the sum of the scenario probabilities over the dam-break scenario ensemble is 1.

Quantitative estimation of the flooding severity in the inundation area is provided by flood hazard maps for each dam-break scenario. Many hydraulic variables are potentially involved in flood hazard assessment, such as maximum flood depth, maximum flow velocity, dam-break wave arrival time, the floodwater rate of rising, and duration of inundation (Merz et al. 2007; de Moel et al. 2015; Maranzoni et al. 2023). In this study, the flood hazard rating is defined according to the DEFRA (2006) classification of the hazard to people, based on the flood hazard index

$$HR = h \cdot (|v| + 0.5) + DF \quad (1)$$

where  $h$  is the flood depth (in m),  $|v|$  is the magnitude of the flow velocity (in m/s), and  $DF$  is a debris factor (depending on flood depth, flow velocity, and land use). In the absence of debris ( $DF=0$ ), flood hazard to people is categorized into four hazard levels as in Table 1 on the basis of the local maximum value of  $HR$ .

Flood hazard mapping requires hydrodynamic inundation modelling to predict the hydraulic quantities involved in flood hazard assessment. Depth-averaged models based on the 2D shallow water equations (SWE) are typically used to this end as they guarantee a valid compromise between accuracy and computational efficiency (Teng et al. 2017; Bates

**Table 1** Flood hazard classes for people, in the absence of debris, according to DEFRA (2006)

Hazard index range	Hazard level	Hazard class, <i>HC</i>	Description
$HR=0$	Residual	0	No danger: no flood zone
$0 < HR < 0.75$	Low	1	Caution: flood zone with shallow flowing water or deep standing water
$0.75 \leq HR < 1.25$	Moderate	2	Danger for some people: flood zone with deep or fast flowing water
$1.25 \leq HR < 2.5$	Significant	3	Danger for most people: flood zone with deep, fast flowing water
$HR \geq 2.5$	Extreme	4	Extreme danger for all people: flood zone with deep, fast flowing water

2022). In this study, the dam-break wave propagation was simulated by a GPU-parallel SWE model, which solves the governing equations on Block Uniform Quadtree (BUQ) multi-resolution structured grids using an explicit second-order accurate Godunov-type finite volume scheme (Vacondio et al. 2017).

## 2.2 Flood exposure

Flood damage maps illustrate the potential adverse consequences caused by a flooding event to human health, buildings, economic activities, and the environment (e.g. Merz et al. 2007; de Moel et al. 2009). This work focuses specifically on the direct risk of life loss. Accordingly, flood exposure is related to the spatial distribution of the population at risk from flooding within the study area.

The basic demographic information is obtained from choropleth maps of population density, usually available from local authorities in digital format. Choropleth maps visualize the distribution of the average population density within the administrative limits of municipalities in a specific region, typically distinguishing urban centres and main settlements from rural areas. A more detailed and accurate description of the spatial distribution of the population, which is more suitable for the scope of the characterization of flood exposure, is provided by dasymetric maps. These can be obtained by overlaying choropleth maps with land use maps and recalculating local population densities on a building or neighbourhood scale excluding uninhabited areas. Inhabited areas can easily be categorized by type from land use maps (e.g. residential areas, industrial and production sites, schools, hospitals, shopping centres, services, farm buildings, etc.).

Different socio-economic states are considered to include epistemic uncertainty inherent in exposure assessment, thereby taking into account the potential variation of the population at risk and its distribution within the study area at different times of the day and week. The dynamics of change in the spatial distribution of the population is mainly dictated (on a daily/weekly basis) by working activities; therefore, two socio-economic states are considered in this study: a ‘business hours’ scenario, which pertains to working weekdays during standard business hours (i.e. 8 am–5 pm), and a ‘non-business hours’ scenario, which encompasses weekdays outside working hours and weekends. The former scenario accounts for 26.8% of the total hours in a standard week, while the latter covers the remaining 73.2%. Therefore, the probabilities of these two socio-economic states are 0.268 and

0.732, respectively. The aleatory uncertainty associated with the spatial distribution of the population at risk at different times is neglected in the analysis.

Flood exposure maps can be obtained for each combination of dam-break scenarios and social states by overlaying hazard information (provided by flood hazard maps) and socio-economic information (provided by dasymetric maps of population density or, if of interest, other maps representing the exposed assets) in order to identify the elements at risk that are actually exposed to flooding (Merz et al. 2007; de Moel et al. 2015).

### 2.3 Flood vulnerability

An empirical vulnerability model derived from statistical analyses of mortality data from historical dam-breaks is used to describe the susceptibility of the population at risk to dam-break flooding in terms of fatality rate (Jonkman et al. 2008).

The flood hazard-loss model expressed in tabular form in Table 2 is adopted in this study. This model, initially proposed by Graham (1999) and subsequently modified by Sun et al. (2014), provides the fatality rate due to dam-break flooding as a function of flood hazard, warning time, and flood severity understanding.

In the hazard-loss relationship outlined in Table 2, flood hazard is categorized into three classes: high, medium, and low hazard. The higher class (corresponding to the greatest flood severity) is assumed to coincide with the ‘extreme’ hazard level of the classification by DEFRA (2006) (Table 1). The ‘significant’ and ‘medium’ hazard levels defined by DEFRA (2006) are merged into the ‘medium’ hazard class of Table 2. Finally, the ‘low’ hazard levels in both classifications are assumed to be equivalent and treated as the same category.

**Table 2** Fatality rate of population at risk due to dam failure (from Sun et al. 2014, modified from Graham 1999)

Flood severity	Warning time (h)	Flood severity awareness	Fatality rate ( <i>FR</i> )	
			Suggested value	Suggested range
High (Hazard level: extreme; <i>HC</i> = 4)	No warning	Not applicable	0.75	0.3–1
	0.25–1	Vague	0.2	0.05–0.4
		Precise	0.001	0–0.002
	> 1	Vague	0.18	0.01–0.3
		Precise	0.0005	0–0.002
	Medium (Hazard levels: signifi- cant and moderate; <i>HC</i> = 3, 2)	No warning	Not applicable	0.5
0.25–1		Vague	0.13	0.015–0.27
		Precise	0.0008	0.0005–0.002
> 1		Vague	0.05	0.01–0.1
		Precise	0.0004	0.0002–0.001
Low (Hazard level: low; <i>HC</i> = 1)		No warning	Not applicable	0.03
	0.25–1	Vague	0.007	0–0.015
		Precise	0.0006	0–0.001
	> 1	Vague	0.0003	0–0.0006
		Precise	0.0002	0–0.0004

Warning time is defined as the difference between the arrival time of the dam-break wave at the population at risk and the warning issue time (i.e. the time when warning would be initiated after the dam failure), which is considered to be different in the day (from 8 a.m. to 10 p.m.) and the night (from 10 p.m. to 8 a.m.) periods. The issuance of dam warning is set here at 0.25 h and 0.5 h after the dam failure for the former and the latter case, respectively, as suggested by Graham (1999) for an immediate dam failure. Table 2 considers three warning time categories: ‘no’ warning, which means that the dam-break flooding wave arrives before any alert is issued or communicated, or with less than 15 min notice; ‘some’ warning time of 0.25–1 h; and ‘adequate’ warning time of more than 1 h before the arrival of the flooding wave (Graham 1999).

As for the last factor affecting the fatality rate, two categories of flood severity understanding are introduced in Table 2: ‘vague’ (unclear) and ‘precise’ (clear) awareness, depending on the distance from the dam (Graham 1999).

The fatality rate range provided in Table 2 along with the suggested (average) value represents the maximum range calculated on the basis of the dataset available from historical dam failures (Graham 1999). In principle, statistical analysis of this dataset could provide a median fatality rate value along with confidence intervals at specific confidence levels. Accordingly, the vulnerability model can be interpreted as a multivariate fragility function describing the uncertainty in the vulnerability hazard-loss model through a selected confidence interval.

## 2.4 Flood damage

Flood damage maps are obtained by combining the vulnerability model with flood hazard and exposure maps (Hartford and Baecher 2004; de Moel et al. 2015).

To quantify the consequences of dam-break flooding in terms of potential casualties, the damage factor—represented here by the fatality rate—needs to be multiplied by the value of elements at risk—here, the local density of the population at risk (de Moel and Aerts 2011). Therefore, a loss-of-life (LOL) flood risk index is defined as

$$R_{LOL} = FR \cdot \bar{\delta}_{PAR} \quad (2)$$

where  $FR$  is the fatality rate (i.e. the expected loss-of-life rate caused by the dam-break flooding), and  $\bar{\delta}_{PAR}$  is the dimensionless population at risk (PAR) density, defined as the ratio of the local PAR density to the maximum population density of both socio-economic scenarios. This index provides a dimensionless and normalized flood damage estimate in terms of the fatality density of the population at risk due to dam-break flooding. The  $R_{LOL}$  index is normalized to 1 for convenience—that is,  $R_{LOL}$  is locally equal to unity if everyone dies (i.e.  $FR = 1$ ) where the population density attains its maximum value in the study area (i.e.  $\bar{\delta}_{PAR} = 1$ ). Conversely,  $R_{LOL}$  is equal to zero (i.e. no flood risk) if the fatality rate is null (i.e.  $FR = 0$ ) or the area is uninhabited (i.e.  $\bar{\delta}_{PAR} = 0$ ).

## 2.5 Probabilistic flood damage maps

After generating flood damage maps for each combination of dam-break scenarios and socio-economic states, and calculating the corresponding compound probabilities (conditional on the dam-break event), probabilistic flood damage maps can be obtained from



statistical analysis. Such probabilistic maps illustrate the effects of uncertainties in the different risk components (flood hazard, exposure, and vulnerability) on the estimated flood damage (in terms of loss of life).

Probabilistic flood damage maps depict the spatial distribution in the flooded area of a ‘probabilistic’ value for the selected damage indicator (here, the loss-of-life risk index  $R_{LOL}$ ) while also considering its associated uncertainty. An effective way of probabilistically quantifying a flood damage is to express it in terms of selected percentiles. For example, the  $X$ th-percentile map of the  $R_{LOL}$  index displays the distribution of the  $R_{LOL}$  value that will not be exceeded in  $X\%$  of cases in the event of a dam failure (Vorogushyn et al. 2010; D’Oria et al. 2019). To obtain this map, the cumulative distribution function of  $R_{LOL}$  must first be constructed for each grid cell of the flooded area. Then, the selected percentile can be calculated for each grid cell from the corresponding cumulative distribution function.

When the vulnerability model is described by a fragility function or when the hazard-loss relationship includes uncertainty bounds, percentile maps of the flood damage indicator can be coupled with maps estimating the uncertainty (due to the vulnerability model) associated with the probabilistic damage predictions. Confidence intervals for the percentile damage estimates can be calculated for each location by considering the extreme values of the confidence interval of the damage (fatality) rate. These intervals can be visualized through two maps that depict the lower and upper limits of the intervals.

By analysing the probabilistic information merged according to temporal and spatial criteria, it is possible to obtain conditional probability distributions of total damage (in terms of loss of life) for the entire flooded area or portions of it in the event of a dam failure at specific times of a weekday or weekend, or a given season (Hartford and Baecher 2004). Such probability distributions can also be associated with confidence intervals, in which the uncertain damage falls with a fixed confidence level.

### 3 Case study

The probabilistic flood damage model was applied to the case study of the hypothetical dam-break of Mignano dam, located in the upper valley of the River Arda, a tributary of the River Po in northern Italy. Figure 2 shows the case study area; highlighted are the dam location, the most populous urban areas, and the main transport infrastructures.

Mignano dam is a concrete gravity structure with a curved planimetric profile and a nearly triangular transverse section, constructed in 1926–1933 primarily for irrigation purposes (ANIDEL 1953). Potable water supply has since been added as a secondary use.

The catchment area at the dam site is 87 km<sup>2</sup>, and the average elevation of the upper watershed is 748 m a.s.l. The 1000-year return period flood peak entering the reservoir was set at 800 m<sup>3</sup>/s by the competent supervisory authority (Belicchi et al. 2008). Previous works by different authors estimated the peak outflow discharge in the event of a total dam collapse with the reservoir level at the spillway crest to be slightly higher than 30,000 m<sup>3</sup>/s (Ferrari et al. 2023; Rizzo et al. 2023). The maximum flow discharge compatible with the conveyance of the downstream river reach is estimated to be 65 m<sup>3</sup>/s (Resolution of the Regional Council of Emilia-Romagna no. 967 of 14 May 2018).

Mignano dam has a height of 51 m measured from the downstream thalweg. The dam crest is situated at 342 m a.s.l. and is 341 m long. The reservoir capacity is approximately

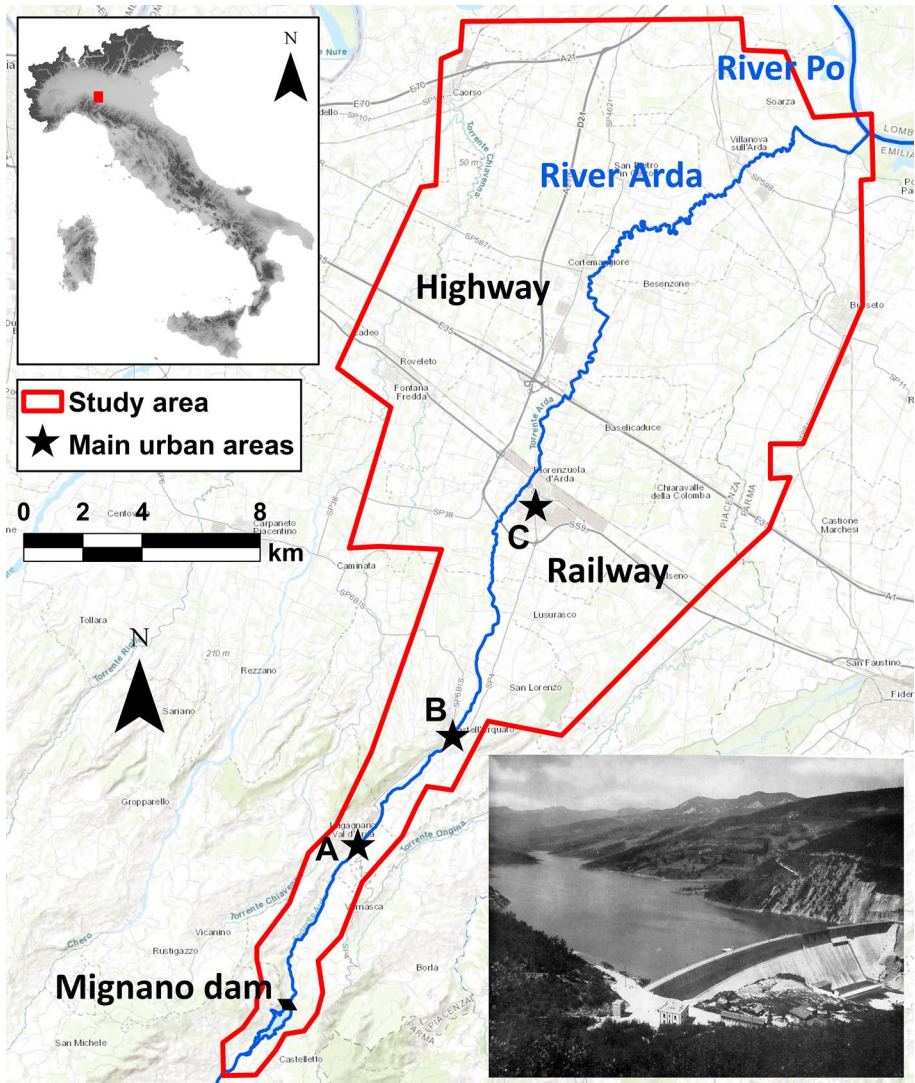


**Fig. 2** Case study area; highlighted are the location of Mignano dam, the main transport infrastructures, and the most populous urban centres (A Lugagnano Val d'Arda; B Castell'Arquato; and C Fiorenzuola d'Arda). Bottom right inset: historical picture of Mignano dam and reservoir (ANIDEL 1953)

15 million  $\text{m}^3$  when the lake is filled to the maximum storage level of 340.5 m a.s.l. (ANIDEL 1953). The dam is equipped with a frontal uncontrolled overflow structure able to evacuate the design 1000-year return period discharge. The spillway is divided into eight sections, each spanning 10.5 m, with the crest at 337.8 m a.s.l.

The hypothetical collapse of Mignano dam poses a severe threat to the downstream valley and floodplain since a large area, rich in natural and historical sites and various economic activities (farms, industries, and services), would be flooded, with potentially

catastrophic consequences. Furthermore, densely populated urban areas, such as Lugagnano Val d'Arda and Castell'Arquato in the Arda valley (3000 and 2400 inhabitants, respectively) and Fiorenzuola d'Arda in the floodplain (13,200 inhabitants), are vulnerable to flooding in the event of a failure of Mignano dam (Fig. 2). Traffic along key transport infrastructures (a national highway and a regional railway), as well as arterial and secondary roads, would be disrupted.

The study area has an extension of 338 km<sup>2</sup> and a population of approximately 49,000 people, as recorded in the 2011 Census, mostly living in urban areas. The average population density is 27.5 inhabitants per square kilometre, with the town of Fiorenzuola reaching the peak of an average density of 3044 inhabitants per square kilometre (Emilia-Romagna Region Geoportal 2021). Dasymeric maps of the population density for the two socio-economic states considered were derived from the choropleth maps of demographic data exploiting the 2014 land cover data (Emilia-Romagna Region Geoportal 2021). To this end, the resident population (estimated at 48,892 people) was firstly redistributed into residential areas to build the 'non-business hours' exposure scenario (weekend, and weekday night). The resulting 'non-business hours' dasymeric map reveals a peak demographic density of approximately 9000 inhabitants per square kilometre in Fiorenzuola. Corrective factors were then applied to estimate the population distribution in the 'business hours' scenario (on a weekday during worktime). These factors include age and employment rate (to calculate the unemployed or inactive population), commuting patterns for work (Gazzola 2015), the number of school pupils (to determine the unemployed population who stay in their homes during the day), the population in service areas (i.e. people employed in services, as well as students and teachers in schools), and the population working in industry and manufacturing. A special treatment was reserved for shopping centres, for which a fixed population density of 4000 inhabitants per square kilometre was assumed during opening hours. Consequently, in the 'business hours' exposure scenario, the estimated total population present in the area during daytime hours is 48,556 people, with a peak density of 41,403 inhabitants per square kilometre in some service areas located in Fiorenzuola. The total population of the two exposure states does not differ substantially (only 336 individuals) because of the reduced net effect of commuting to and from the study area. Seasonal fluctuations due to tourism are negligible in this area.

In the hydrodynamic model of the study area, the computational domain was discretized by a high-resolution BUQ grid generated from a 1 m × 1 m digital elevation model (DEM) based on Lidar data. Four different spatial resolutions were adopted in the BUQ grid (Fig. 3a), with cell size progressively increasing by a factor of 2. The smallest cells (with a size of 2 m) were used to accurately describe the lowest part of the valley and the course of the River Arda. Areas near the main infrastructures were discretized with 4 m squared cells to accurately reproduce the effects of linear structures or embankments (assumed non-erodible) which can act as barriers to flooding. Finally, cells with sizes of 8 and 16 m were used in the highest part of the Arda valley sides (not expected to be swept by the dam-break wave) and in large areas of the floodplain, where a lower spatial resolution is sufficient given the flat topography. The Manning roughness coefficient was set at values ranging from 0.033 to 0.083 m<sup>-1/3</sup> s along the course of the River Arda (depending on the river conditions), at 0.05 m<sup>-1/3</sup> s along the sides of the valley and in the floodplain, and 0.02 m<sup>-1/3</sup> s in the urban areas and along the main roads (Fig. 3b). The predicted maximum flooding extent after a 4-h simulation was considered to identify the flood inundation area on which to evaluate the population at risk.

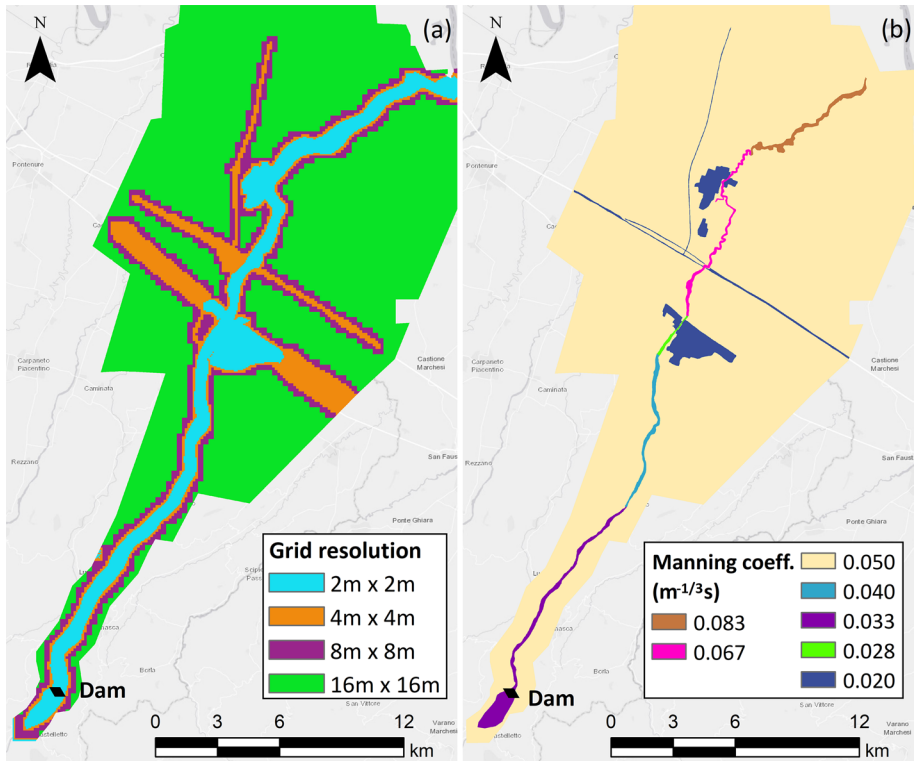


**Fig. 3** Two-dimensional shallow water hydrodynamic model: **a** spatial resolutions of the BUQ computational grid; **b** spatial distribution of the Manning roughness coefficient

## 4 Results

### 4.1 Flood hazard maps

A set of 20 dam-break scenarios, defined by combining five representative reservoir levels with four breach widths, were considered for the Mignano dam-break case study (see Rizzo et al. 2023 for details). The probabilities conditional on the dam failure associated with the selected dam-break scenarios were determined assuming the breach width and the reservoir level as independent stochastic variables. The marginal probabilities for these two variables were estimated through frequency analyses of historical data on breach width for concrete and masonry dams, and on water level recorded daily from 1934 to 2019 for Mignano reservoir (Rizzo et al. 2023). In this study, dam-break scenario probabilities were differentiated according to two seasons, i.e. autumn–winter and spring–summer. To this end, we calculated two separate empirical cumulative frequency functions of the daily reservoir water levels for the two seasons considered. The dam-break scenarios and the associated conditional probabilities are shown in Table 3.

Flood hazard maps were produced for each dam-break scenario. As an example, Fig. 4 shows the maps for the most catastrophic scenario, characterized by the total collapse of the dam when the upstream reservoir is at its maximum level. In particular, Fig. 4a depicts

**Table 3** Probabilities (conditional on the dam-break event) of the selected dam-break scenarios for the Mignano dam case study (from Rizzo et al. 2023)

	Breach width				Total
	$L_0 = 340.4$ m	$L_1 = 243.0$ m	$L_2 = 169.2$ m	$L_3 = 82.5$ m	
Water level $H_0 = 340.5$ m a.s.l. (full reservoir level)	0.0208 (0.0034, 0.0174)	0 (0, 0)	0.0520 (0.0084, 0.0436)	0.0937 (0.0152, 0.0785)	0.1665 (0.0270, 0.1395)
$H_1 = 337.8$ m a.s.l. (spillway crest level)	0.0082 (0.0033, 0.0049)	0 (0, 0)	0.0206 (0.0082, 0.0124)	0.0371 (0.0148, 0.0223)	0.0659 (0.0263, 0.0396)
$H_2 = 336.5$ m a.s.l. (first civil protection alert level)	0.0299 (0.0148, 0.0151)	0 (0, 0)	0.0747 (0.0370, 0.0377)	0.1343 (0.0665, 0.0678)	0.2389 (0.1183, 0.1206)
$H_3 = 330$ m a.s.l.	0.0257 (0.0116, 0.0141)	0 (0, 0)	0.0643 (0.0292, 0.0351)	0.1158 (0.0525, 0.0633)	0.2058 (0.0933, 0.1125)
$H_4 = 320$ m a.s.l.	0.0404 (0.0265, 0.0139)	0 (0, 0)	0.1009 (0.0663, 0.0346)	0.1816 (0.1193, 0.0623)	0.3229 (0.2121, 0.1108)
Total	0.1250 (0.0596, 0.0654)	0 (0, 0)	0.3125 (0.1491, 0.1634)	0.5625 (0.2683, 0.2942)	1 (0.4770, 0.5230)

Distinct probabilities depending on season (autumn–winter and spring–summer) are reported in brackets

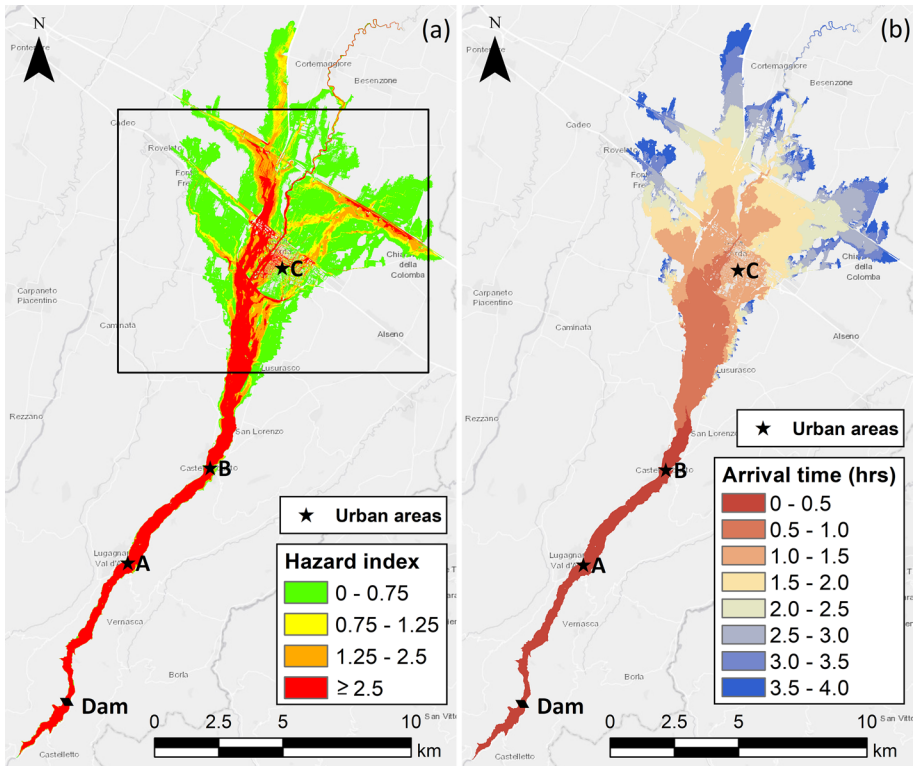


**Fig. 4** Flood hazard maps for the most catastrophic scenario (total collapse of the dam with the reservoir at its maximum level): **a** map of the flood hazard index (the box indicates a zoom area for the following figures), and **b** map of the flood wave arrival time

the flood hazard index map according to the classification reported in Table 1 (DEFRA 2006). According to this map, the highest flood hazard level for the considered scenario is concentrated along the valley of the River Arda and in a region on the left-hand side of the watercourse within the floodplain. The embankments of the transport infrastructures, which cross the floodplain acting as flow barriers, contribute to increasing the flood depth, and consequently the hazard level. The flood hazard decreases towards the boundaries of the flooded area, reaching the ‘low’ hazard level in large areas of the alluvial fan, where the flooding expands, reducing its velocity. Figure 4b is the map of the flood arrival time for the same catastrophic scenario. This map shows that the dam-break wave sweeps the entire valley downstream of the dam in less than 30 min and reaches the most populous city in the study area (Fiorenzuola, point C in the figure) in approximately 1 h.

### 4.2 Flood exposure maps

Considering people as the only element at risk, flood exposure is described through the spatial distribution of the population in the area downstream of the dam.

Figure 5 shows flood exposure maps of the population at risk for the two socio-economic states considered: the ‘business hours’ scenario (Fig. 5a) for weekdays during

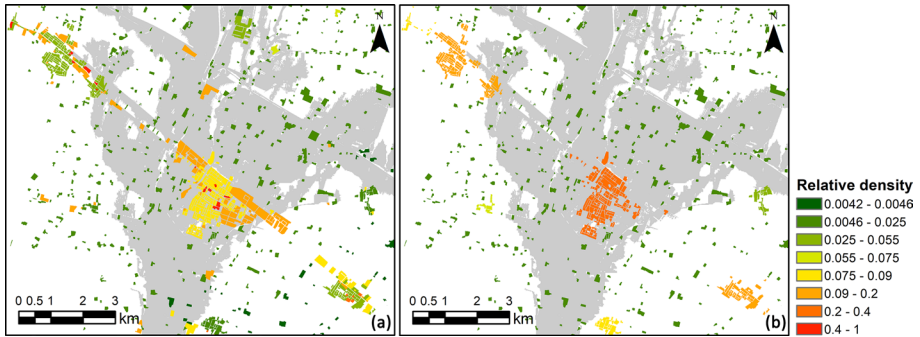


**Fig. 5** Flood exposure maps: density of the population at risk in **a** ‘business hours’ and **b** ‘non-business hours’ socio-economic scenarios. Density is expressed in a non-dimensional form by dividing it by the maximum population density within the area. The maps are restricted to the region delimited by the box in Fig. 4a for clarity’s sake. The grey shadow indicates the envelope of the flooded areas across all the dam-break scenarios

business hours (i.e. 8 a.m.–5 p.m.) and the ‘non-business hours’ scenario (Fig. 5b) for weekends and weekdays outside working hours (i.e. 5 p.m.–8 a.m.). The population density is expressed in a dimensionless form by dividing it by the peak population density estimated within the area. For clarity’s sake, Fig. 5 contains zooms of the flood exposure maps limited to the area in the alluvial fan indicated by the box in Fig. 4a. The dasymetric maps of the density of the population at risk are superimposed on the flood inundation map, which identifies the boundaries of the envelope of the flooded areas across all the dam-break scenarios. The population within these boundaries is at risk of flooding in the event of a dam failure. In the case study analysed, the population density is highly variable in the urban areas in the ‘business hours’ scenario, with the population being distributed in commercial, service, industrial, manufacturing, and residential areas (Fig. 5a). During night time and at weekends (‘non-business hours’ scenario), the population is concentrated in residential areas with a nearly uniform density (Fig. 5b).

### 4.3 Flood vulnerability

The vulnerability of people exposed to dam-break flooding was quantified via the empirical flood hazard-damage function outlined in Table 2. Maps depicting the spatial distribution of the fatality rate were generated using this vulnerability model for each dam-break scenario and both socio-economic states considered. To this end, flood hazard maps (Fig. 4a) were exploited to estimate flood severity and arrival time maps (Fig. 4b) in order to predict warning time; flood severity awareness was assumed to be vague in the valley and precise in the floodplain. The fatality rate maps are not shown here for brevity.

### 4.4 Flood damage maps

Combining flood exposure maps with fatality rate maps allows the calculation of flood damage maps. Such maps depict the spatial distribution of the loss-of-life risk index ( $R_{LOL}$ ), which serves as an indicator of potential dam-break flooding damage in terms of life loss. Accordingly, such maps show the spatial variation of the dimensionless areal density of

loss of life within the potentially flooded area for each combination of dam-break scenarios with socio-economic states.

A total of 40 composite scenarios were considered from the combination of 20 dam-break scenarios (characterized by different breach widths and reservoir levels) with two socio-economic states (characterized by different spatial distributions of the population at risk). Each composite scenario was assigned a compound probability (conditional on the dam failure), calculated by multiplying the conditional probability of a dam-break scenario and the probability of a socio-economic state, according to the theorem of compound probability for independent events.

As an example, Fig. 6 shows zooms of the flood damage maps for the most catastrophic scenario (total collapse of the dam with the reservoir at its maximum level) for the two socio-economic states considered.

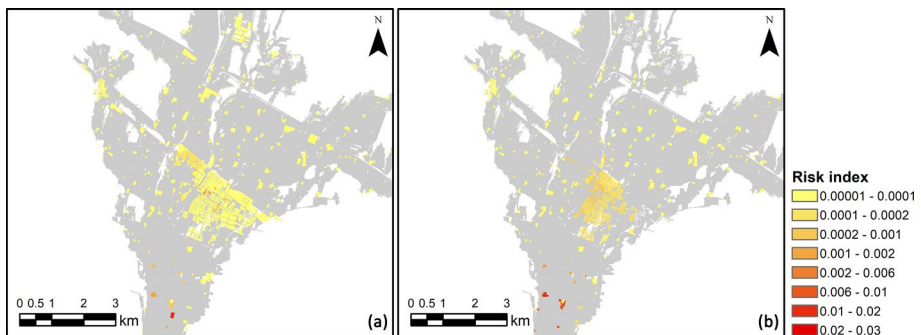
## 4.5 Probabilistic flood damage assessment

### 4.5.1 Probabilistic flood damage maps

The maps resulting from damage mapping for each composite scenario were statistically analysed using the associated compound probabilities to generate probabilistic flood damage maps. Percentile maps of the loss-of-life risk index ( $R_{LOL}$ ) provide a probabilistic quantitative information on the uncertainty associated with flood damage assessment (in terms of loss of life).

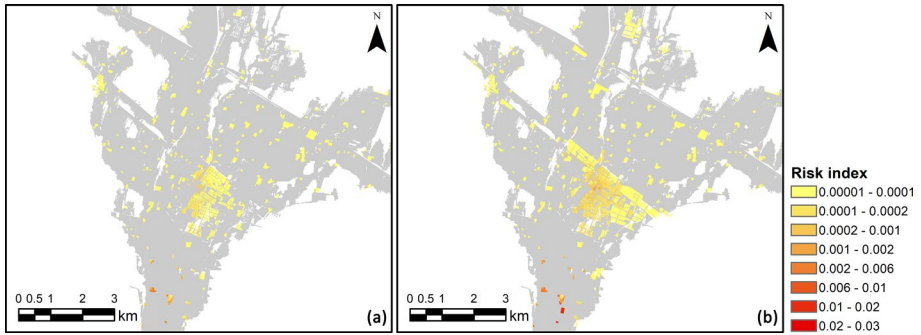
Figure 7 shows the 50th- and 90th-percentile maps of the loss-of-life risk index,  $R_{LOL}$ , for a selected portion of the study area. For each location, these maps provide the values of  $R_{LOL}$  that are expected to be exceeded in 50% and 10% of cases, respectively, in the event of a dam failure. Maps corresponding to different percentiles show different patterns. In particular, in higher-percentile maps, the risk area (in which  $R_{LOL} > 0$ , i.e. there is a non-null risk of loss of life) is larger, and the global risk for the population potentially affected is higher, as expected.

Figure 8a shows the 99th-percentile map of the  $R_{LOL}$  index obtained using the values of the fatality rate suggested in the vulnerability model in Table 2. Figure 8b and c shows the maps of the lower and upper limits, respectively, of the confidence interval associated with



**Fig. 6** Flood damage maps: loss-of-life risk index for the most catastrophic scenario (total collapse of the dam with the reservoir at its maximum level) in the **a** 'business hours' and **b** 'non-business hours' socio-economic scenarios. The maps are restricted to the region delimited by the box in Fig. 4a for clarity's sake. The grey shadow indicates the envelope of the flooded areas across all the dam-break scenarios





**Fig. 7** Probabilistic flood risk maps: **a** 50th and **b** 90th percentile of the loss-of-life risk index. The maps are restricted to the region delimited by the box in Fig. 4a for clarity’s sake. The grey shadow indicates the envelope of the flooded areas across all the dam-break scenarios

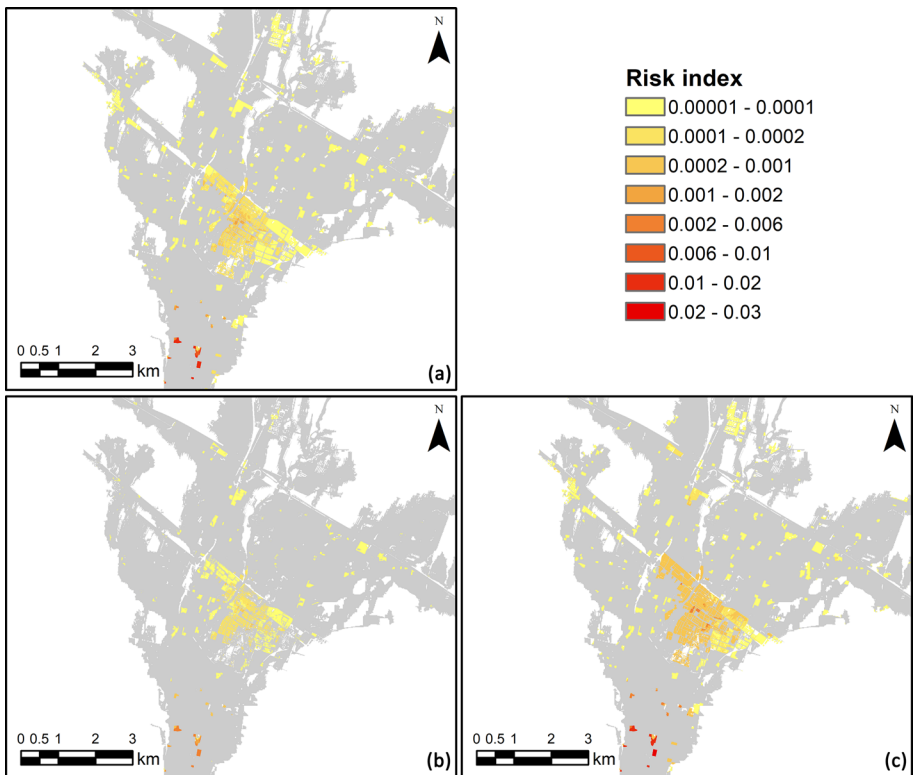


**Fig. 8** Probabilistic flood risk maps: **a** 99th percentile of the loss-of-life risk index. Uncertainty in probabilistic flood hazard mapping: confidence interval for the 99th percentile of the loss-of-life risk index: **b** lower limit; **c** upper limit. The maps are restricted to the region delimited by the box in Fig. 4a for clarity’s sake. The grey shadow indicates the envelope of the flooded areas across all the dam-break scenarios

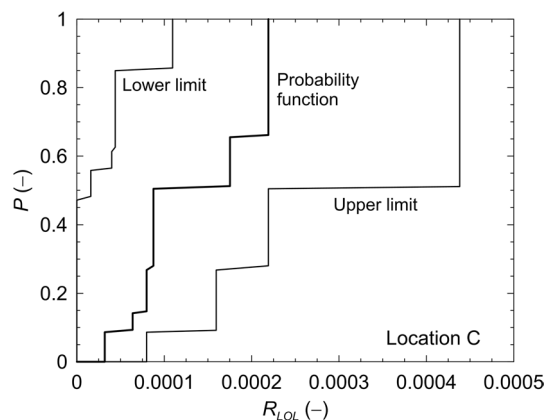
the 99th percentile of the loss-of-life risk index. These maps (Fig. 8b and c) were obtained from the extreme values of the fatality rate ranges reported in Table 2 and provide uncertainty bounds (reflecting the uncertainty in the vulnerability model) for the probabilistic local estimates of the flood risk indicator (which incorporate uncertainties in dam-break scenarios and flood exposure).

#### 4.5.2 Loss-of-life probability distributions

Cumulative distribution functions of the loss of life risk index,  $R_{LOL}$ , can be extracted in selected locations from the flood damage maps by considering the entire set of composite scenarios originated from the combination of dam-break scenarios with socio-economic states along with the associated (conditional) compound probabilities. For example, Fig. 9 shows the cumulative distribution function of  $R_{LOL}$  for point C located in the urban area of Fiorenzuola (Fig. 2). The associated uncertainty bounds were determined by calculating cumulative distribution functions with the extreme values of the suggested fatality rate range in the vulnerability model (Table 2). In point C, the 99th percentile of the  $R_{LOL}$  index is  $2.2 \times 10^{-4}$  with an asymmetric confidence interval of approximately  $3.2 \times 10^{-4}$ ; the maximum percentage variation is about 100%.

Integral probabilistic information about the potential loss of life in delimited regions of the study area can also be obtained from the statistical analysis of flood damage maps with associated probabilities. Figure 10a shows the cumulative distribution function of loss of life (along with the associated uncertainty bounds) for the entire flood inundation area. The population at risk is estimated to be 17,156 people in the ‘business hours’ socio-economic scenario, and 15,021 people in the ‘non-business hours’ scenario, out of approximately 49,000 people living in the study area. According to Fig. 10a, the 90th percentile of fatalities across the entire inundation area (envelope of the flooded areas across all the dam-break scenarios) is 1443, with a confidence interval of [565, 1967]. The total casualties should not exceed 1616, with a confidence interval of [624, 2198]. Figure 10b shows the probability distributions of loss of life (along with the associated confidence interval) for two different sub-zones of the study area: the valley and the floodplain. As illustrated in Fig. 10b, in the case study considered the majority of casualties can be expected to occur in the valley, regardless of the dam-break or socio-economic scenario. Despite the relatively low population density, the flood hazard level reached in this zone during dam-break

**Fig. 9** Cumulative distribution function of loss-of-life risk index ( $R_{LOL}$ ) for a selected location along with the associated confidence interval



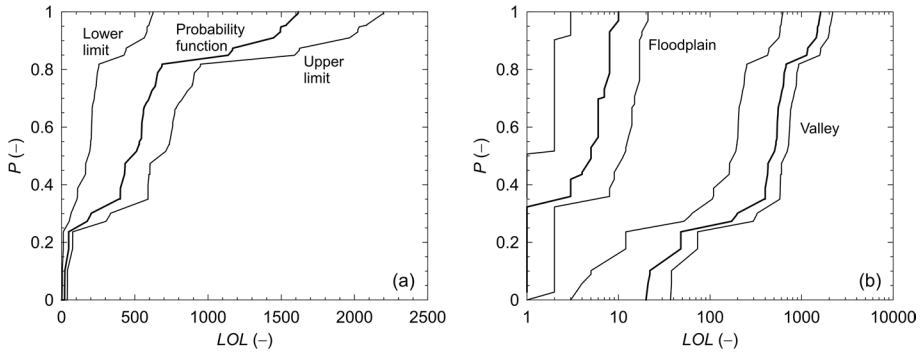


**Fig. 10** Cumulative distribution functions of loss of life (*LOL*): **a** across the entire flooded area; **b** separately for the valley and floodplain, along with the associated confidence intervals

flooding is indeed high, the warning time very short or even null, and the awareness of the dam-break flood severity quite vague. The fatalities would certainly not exceed 1608 (with a confidence interval of [623, 2180]) in the valley, and 10 (with a confidence interval of [3, 21]) in the floodplain.

Similarly, probabilistic loss-of-life information can be obtained for the entire study area or its sub-regions by considering distinct time conditions, including different seasons (Fig. 11). However, if the approach of temporally fixing the dam-break flooding event (at certain hours of the day, on a day of the week, or a season) is adopted, it is convenient to build the cumulative distribution function using probabilities conditional on the particular time condition selected. This choice implies that, within the time condition selected, and given a cumulative probability, the corresponding loss-of-life (*LOL*) value is expected not to be exceeded with that probability. For this reason, all the lines in Fig. 11 reach the unit value. In order to differentiate cumulative distribution functions between different seasons, the dam-break scenario probabilities must be separately calculated for the seasons considered, as in Table 3, where the autumn–winter and spring–summer seasons are considered. Figure 11a shows the cumulative distribution function of life loss for the entire study area along with the associated confidence interval if the dam-break occurs during the autumn–winter season, specifically on a weekday during business hours (i.e. 8 a.m.–5 p.m.). Similarly, Fig. 11b depicts the cumulative distribution function along with the associated confidence interval for a dam-break occurring during a weekend between 8 a.m. and 10 p.m. in the autumn–winter season. In this season, if a dam-break occurs during weekdays in working hours, at least 400 casualties are to be expected, regardless of the dam-break or socio-economic scenario; the 99th percentile of *LOL* would be 1615 with a confidence interval of [624, 2197] (Fig. 11a). On the other hand, if a dam-break occurs in daytime hours during a weekend in the autumn–winter season, the 99th percentile of *LOL* would be 640 with a confidence interval of [237, 892] (Fig. 11b). This comparison allows us to conclude that a collapse of Mignano dam in daylight hours on a weekday in the autumn–winter season would be more damaging in terms of life loss than on a weekend. This conclusion is confirmed in Fig. 11c, which compares the cumulative distribution function of loss of life during weekday business hours (i.e. 8 a.m.–5 p.m.) with those obtained in non-working hours (during weekdays or weekends) in two distinct time periods: 5 p.m.–10 p.m. and 10 p.m.–8 a.m. This differentiation is related to the assumed change in warning issue time at 10 p.m. The analysis was conducted again for the autumn–winter season, as an example. It can be observed that the highest percentile values of casualties occur in the case of a

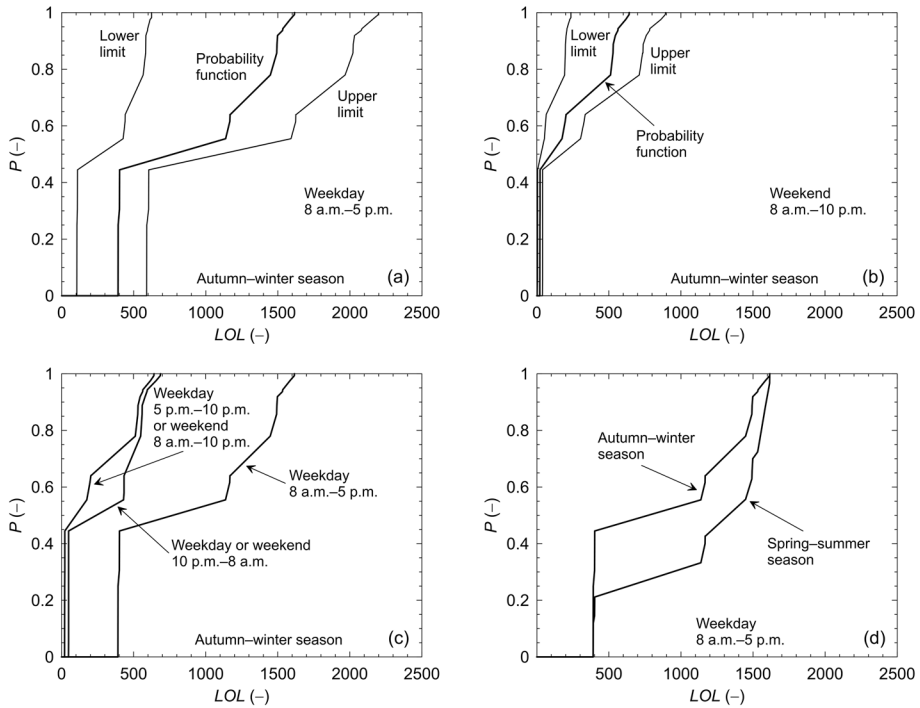


**Fig. 11** Conditional cumulative distribution functions of loss of life (*LOL*) for different temporal conditions: **a** weekday in the autumn–winter season during business hours (along with the confidence interval); **b** weekend in the autumn–winter season during daily hours (along with the confidence interval); **c** weekday in the autumn–winter season at different times during the day; **d** weekday (during business hours) in the autumn–winter and spring–summer seasons

dam-break happening during working hours, while the lowest percentile values are related to the 5 p.m. to 10 p.m. period. It is worth noting that the results obtained for weekdays between 10 p.m. and 8 a.m. are also applicable to weekends during the same period. Similarly, the results obtained for weekdays from 5 p.m. to 10 p.m. are also valid for weekends between 8 a.m. and 10 p.m. Finally, Fig. 11d compares the cumulative distribution functions of loss of life for dam-break flooding occurring during weekdays in business hours in two different seasons: autumn–winter and spring–summer. This comparison shows that, if a certain number of casualties is fixed, it is more probable that this number is exceeded in the spring–summer than in autumn–winter. The two cumulative distribution functions start to differ from around the 20th percentile onwards, with the spring–summer season showing higher *LOL* percentile values. Both curves reach a maximum of 1616 casualties, corresponding to the fatalities expected for the most catastrophic scenario, regardless of the season.

## 5 Discussion

The advantages and limitations of the proposed probabilistic method for dam-break damage assessment are discussed in this section.

- (a) The method is based on the preselection of a set of representative dam-break and socio-economic scenarios. The number of predetermined scenarios and their location in the space of the input variables affect the accuracy of the model results in terms of damage uncertainty and the capability of the model to cover a wide range of flooding consequences (Hartford and Baecher 2004). Model convergence is a challenging issue, worthy of further investigation in the future research, along with the identification of a balanced compromise between model convergence and computational efficiency.
- (b) Considering scenario probabilities conditional on a dam-break event hinders the possibility of comparing the consequences of different dam-break case studies. To enable this comparison, dam-break scenarios should be assigned absolute probabilities as a measure of the frequency of the hazardous events. Accordingly, the probability of the dam collapse for a specific failure mechanism should be calculated for the dams compared.
- (c) The spatial resolution of the flood inundation hydrodynamic model must be adequate for the scope and requirements of the damage analysis (Hartford and Baecher 2004). In general, the use of high-resolution models is desirable to carefully resolve near-field flow features and obtain accurate numerical results. However, high-resolution models are computationally expensive and require handling large amounts of topographic data. The model parallelization significantly increases computational efficiency, thereby allowing high-resolution simulations of a large number of scenarios to be performed in an acceptable computational time. An alternative approach to this problem could be the use of metamodels (Kalinina et al. 2020, 2021). In general, the complexity of the hydrodynamic model (as well as the vulnerability model) should be calibrated to provide a good compromise between computational effort and accuracy of results (Apel et al. 2009).
- (d) The aleatory uncertainties in the total number of inhabitants potentially affected by dam-break flooding and the spatial distribution of the population at risk in the study area were neglected. Instead, the focus was on capturing the epistemic uncertainty associated with the spatial distribution of the exposed population, which varies at different times of the day and days of the week. This uncertainty was addressed by considering socio-economic scenarios with associated probabilities representing the likelihood of the element at risk (people) being present in each location with a specific density during the hazardous event. The choice of the number of representative socio-economic scenarios depends on the specific demographic and economic characteristics of the study area. For example, in areas with significant tourist activity, the seasonal fluctuations in the population potentially at risk cannot be disregarded.
- (e) Flood exposure was considered essentially static during the flooding. However, exposure of people to flood reasonably varies dynamically during the flooding event, even when it is impulsive, like a dam-break. Dynamic exposure maps may describe this temporal variability (Balisticocchi et al. 2020), possibly considering the evacuation/sheltering potential of the population at risk (Ge et al. 2022). In general, early warning systems, evacuation plans, and population preparedness positively affect emergency management, thereby significantly reducing the potential for loss of life (e.g. Lumbroso et al. 2021; Silva and Eleutério 2023b).
- (f) Flood exposure is in constant evolution and can vary in the medium- and long-term due to new urbanizations and changes in demographics and land use in the study area (e.g. de Moel et al. 2011). Accordingly, flood exposure and damage maps must be constantly updated.

- (g) The damaging effect of a dam-break event on the element at risk considered (people) was assessed via a vulnerability model consisting in an empirical flood hazard-damage function. The adequacy of the vulnerability model should be carefully analysed. It is plausible that the vulnerability model needs to be adjusted so as to be aligned with the geographic location of the study area and the flood response policy, particularly the effectiveness of prevention, preparation, and information actions carried out on the population. The effects of possible evacuation and shelter strategies should be incorporated in empirical vulnerability models (Ge et al. 2022). Standardized multivariate fragility functions should be made available to soundly characterize probabilistic vulnerability (Nofal and van de Lindt 2022).
- (h) In empirical vulnerability models, flood severity is typically described qualitatively using categories such as high, medium, and low hazard. This categorization is determined through a qualitative description of the potentially damaging effects of the inundation (e.g. Graham 1999). However, the definition of flood hazard categories based on quantitative flood hazard indexes to evaluate potential adverse consequences is not a trivial matter and requires expert judgement. Indeed, there is a genuine risk of introducing a certain level of arbitrariness when making this assessment.
- (i) Damage estimates obtained via empirical vulnerability models are expected to be influenced by uncertainty in warning time caused by delays in issuing and diffusing the alert (Mileti and Sorensen 2015).
- (j) Probabilistic maps are the main outcome of the probabilistic method. Such maps (based on multiple scenarios) are more informative than the deterministic ones (typically based on a single scenario) and provide flood damage information coupled with an estimate of the associated uncertainty. This comprehensive information assists in prioritizing interventions and comparing alternative mitigation options; revising EAPs; increasing monitoring actions and informative campaigns to improve people preparedness in facing a dam-break event; and planning and executing adaptation works to increase people safety. However, probabilistic mapping requires complicated analyses, and probabilistic maps are more complex to read and interpret. Indeed, their content is not of immediate understanding as the probabilistic damage information cannot be included in a single map.

## 6 Conclusions

This article has shown how probabilistic methods, widely used in the literature and practice for flood hazard and risk assessment in areas potentially subject to flooding due to levee breaches, can also be proficiently adopted in dam-break flood risk assessment to quantify the uncertainty in dam-break flood damage estimate. Indeed, probabilistic methods can include the uncertainties inherent in the main risk components which contribute to the final damage estimate, i.e. hazard, exposure, and vulnerability.

The probabilistic model proposed combines uncertainties in all three components of damage, thereby allowing a higher level flood damage assessment compared to conventional deterministic models, which are unable to provide information about the uncertainty associated with flood damage estimates since they are based on a single (worst) dam-break scenario coupled with a fixed hazard-loss function.

A set of potential dam-break scenarios, differing in terms of breach width and reservoir level, was considered to account for the uncertainty in dam-break flood hazard. Each

scenario was associated with a probability assumed to be conditional on the occurrence of the dam-break event. Since the population living downstream of a dam is the main element at risk in the event of a dam failure, population density dasymmetric maps were used to describe flood exposure. Uncertainty in flood exposure was related to different spatial distributions of the population at risk (having different likelihoods of occurrence), depending on the time of day or day of the week of the hypothetical dam collapse. Finally, flood vulnerability was expressed through an empirical hazard-loss function, and quantitative information about uncertainty underlying flood vulnerability was included in the probabilistic model through uncertainty bounds, which can be interpreted as confidence intervals in which the damage prediction falls with a given confidence level.

A case study concerning the hypothetical collapse of an existing concrete gravity dam (Mignano dam, northern Italy) was used to show the potentialities of the method and verify its advantages and limitations.

The outcome of the probabilistic dam-break damage model consists in probabilistic flood damage maps providing the spatial distribution of selected percentiles of a suitable flood risk index (here, related to loss of life) coupled with the maps of the extreme values of the associated confidence intervals. Statistical analysis of the damage maps combined with the associated probabilities allowed us to obtain (a) probability distributions of the loss-of-life risk index in selected locations and (b) probability distributions of the total casualties expected in the flooded area or its portions due to dam-break events occurring under specific time conditions.

By providing comprehensive information about the uncertainty associated with dam-break flood damage estimates, the probabilistic approach enables more informed decisions in risk-based flood risk management and more accurate cost–benefit analyses than the usual deterministic approach. Albeit more complex and less easy to interpret than the deterministic ones, the probabilistic maps are more informative and may help authorities and stakeholders to take more targeted measures to control risk factors, allocate economic resources more effectively, and prioritize interventions in emergency and risk mitigation planning, thereby improving the effects of risk management and reduction.

**Acknowledgements** The Piacenza Land Reclamation Consortium (Italy) is kindly acknowledged for providing the series of daily water levels measured in Mignano reservoir.

**Author contributions** All authors contributed to the conception and design of the study and to the data collection and analysis. All authors have read and approved the final manuscript.

**Funding** Open access funding provided by Università degli Studi di Parma within the CRUI-CARE Agreement. This work was supported by the Italian Ministry of University and Research through the PRIN 2017 Project RELAIID “REnaissance of LARge Italian Dams”, Project No. 2017T4JC5K.

## Declarations

**Conflict of interest** The authors declare that they have no conflict of interest.

**Open Access** This article is licensed under a Creative Commons Attribution 4.0 International License, which permits use, sharing, adaptation, distribution and reproduction in any medium or format, as long as you give appropriate credit to the original author(s) and the source, provide a link to the Creative Commons licence, and indicate if changes were made. The images or other third party material in this article are included in the article’s Creative Commons licence, unless indicated otherwise in a credit line to the material. If material is not included in the article’s Creative Commons licence and your intended use is not permitted by statutory regulation or exceeds the permitted use, you will need to obtain permission directly from the copyright holder. To view a copy of this licence, visit <http://creativecommons.org/licenses/by/4.0/>.

## References

- Aboelata MA, Bowles DS (2005) LIFESim: a model for estimating dam failure life loss. Report to Institute for Water Resources, US Army Corps of Engineers and ANCOLD by the Institute for Dam Safety Risk Management, Utah State University, Logan, UT. <https://citeseerx.ist.psu.edu/viewdoc/download?doi=10.1.1.74.4264&rep=rep1&type=pdf> Accessed 18 July 2023
- ANIDEL (Italian Association of the Electricity Distribution Companies) (1953) Le dighe di ritenuta degli impianti idroelettrici italiani [Dams of the Italian hydroelectric plants]. ANIDEL, Milan, vol. VII, pp 223–233 (in Italian)
- Apel H, Thielen AH, Merz B, Blöschl G (2004) Flood risk assessment and associated uncertainty. *Nat Hazards Earth Syst Sci* 4(2):295–308. <https://doi.org/10.5194/nhess-4-295-2004>
- Apel H, Aronica GT, Kreibich H, Thielen AH (2009) Flood risk analyses—how detailed do we need to be? *Nat Hazards* 49(1):79–98. <https://doi.org/10.1007/s11069-008-9277-8>
- ASDSO (Association of State Dam Safety Officials) (2023) Emergency action planning. <https://damsafety.org/dam-owners/emergency-action-planning>. Accessed 14 July 2023
- Asselman NEM, Jonkman SN (2003) Consequences of floods: the development of a method to estimate the loss of life. Report DC1-233-7. Delft Cluster. <https://repository.tudelft.nl/islandora/object/uuid:bdf37d5f-18fa-4059-8846-2b781b098340/datastream/OBJ/download>. Accessed 18 July 2023
- Aureli F, Maranzoni A, Petaccia G (2021) Review of historical dam-break events and laboratory tests on real topography for the validation of numerical models. *Water* 13(14):1968. <https://doi.org/10.3390/w13141968>
- Balisticchi M, Metulini R, Carpita M, Ranzi R (2020) Dynamic maps of human exposure to floods based on mobile phone data. *Nat Hazards Earth Syst Sci* 20(12):3485–3500. <https://doi.org/10.5194/nhess-20-3485-2020>
- Bates PD (2022) Flood inundation prediction. *Annu Rev Fluid Mech* 54(1):287–315. <https://doi.org/10.1146/annurev-fluid-030121-113138>
- Belicchi M, Cerlini D, Majone U, Fiorotto V, Volpe F (2008) La ristrutturazione della diga di Mignano [Mignano dam rehabilitation]. *L'Acqua* 6/2008:17–31 (in Italian). <https://www.studiomajone.it/wp-content/uploads/2015/09/BELICCHI-N.-6-2008.pdf>. Accessed 4 July 2023
- Beven K, Lamb R, Leedal D, Hunter N (2015) Communicating uncertainty in flood inundation mapping: a case study. *Int J River Basin Manag* 13(3):285–295. <https://doi.org/10.1080/15715124.2014.917318>
- Beven KJ, Almeida S, Aspinall WP, Bates PD, Blazkova S, Borgomeo E et al (2018) Epistemic uncertainties and natural hazard risk assessment – Part 1: a review of different natural hazard areas. *Nat Hazards Earth Syst Sci* 18(10):2741–2768. <https://doi.org/10.5194/nhess-18-2741-2018>
- Bowles DS, Aboelata M (2006) Evacuation and life-loss estimation model for natural and dam break floods. In: Vasiliev O, van Gelder P, Plate E, Bolgov M (eds) *Extreme hydrological events: new concepts for security*. NATO Science Series, vol 78. Springer, Dordrecht, pp 363–383
- Cardona OD, van Aalst MK, Birkmann J, Fordham M, McGregor G, Perez R, Pulwarty RS, Schipper ELF, Sinh BT (2012) Determinants of risk: exposure and vulnerability. In: Field CB, Barros V, Stocker TF, Qin D, Dokken DJ, Ebi KL, Mastrandrea MD, Mach KJ, Plattner G-K, Allen SK, Tignor M, Midgley PM (eds) *Managing the risks of extreme events and disasters to advance climate change adaptation. A special report of working Groups I and II of the Intergovernmental Panel on Climate Change (IPCC)*. Cambridge University Press, Cambridge, UK, pp 65–108. [https://www.ipcc.ch/site/assets/uploads/2018/03/SREX-Chap2\\_FINAL-1.pdf](https://www.ipcc.ch/site/assets/uploads/2018/03/SREX-Chap2_FINAL-1.pdf) Accessed 18 July 2023
- CDSO (Indian Central Dam Safety Organisation) (2018) Guidelines for mapping flood risks associated with dams. Document no. CDSO\_GUD\_DS\_05\_v1.0. Central Water Commission, New Delhi. [https://damsafety.cwc.gov.in/ecm-includes/PDFs/Guidelines\\_for\\_Mapping\\_Flood\\_Risks\\_Associated\\_with\\_Dams.pdf](https://damsafety.cwc.gov.in/ecm-includes/PDFs/Guidelines_for_Mapping_Flood_Risks_Associated_with_Dams.pdf). Accessed 5 July 2023
- CEIWR-HEC (2020) HEC-LifeSim Life loss estimation. Technical reference manual. Version 2.0. US Army Corps of Engineers, Davis, CA. <https://publibrary.planusace.us/document/c1dae7c1-c83f-4e9d-82e9-f311fa67f2ef>. Accessed 18 July 2023
- Chanson H (2004) *Environmental hydraulics of open channel flows*. Elsevier, Oxford
- Circular from the Italian Prime Minister 13.12.1995, n. DSTN/2/22806 (1995) Raccomandazioni per la mappatura delle aree a rischio di inondazione conseguente a manovre degli organi di scarico o ad ipotetico collasso delle dighe [Recommendations for the mapping of areas at risk of flooding following manoeuvres of dam spillways and outlets or hypothetical collapse of dams] (in Italian). [https://dgdighe.mit.gov.it:5001/\\$DatiCmsUtente/normativa/direttive\\_circolari/1995\\_Circ\\_PCM-13-12\\_n\\_DSTN-2-22806-Raccomandazioni.pdf](https://dgdighe.mit.gov.it:5001/$DatiCmsUtente/normativa/direttive_circolari/1995_Circ_PCM-13-12_n_DSTN-2-22806-Raccomandazioni.pdf). Accessed 18 Oct 2023



- Costa JE (1985) Floods from dam failures. Open-File Report 85–560. US Department of the Interior, Geological Survey, Denver, CO. <https://pubs.er.usgs.gov/publication/ofr85560>. Accessed 21 April 2022
- DEFRA Environment Agency (2006) Flood risks to people. FD2321/TR2 Guidance Document. Department for Environment, Food and Rural Affairs, London. [https://assets.publishing.service.gov.uk/media/602bbc3de90e07055f646148/Flood\\_risks\\_to\\_people\\_-\\_Phase\\_2\\_Guidance\\_Document\\_Technical\\_report.pdf](https://assets.publishing.service.gov.uk/media/602bbc3de90e07055f646148/Flood_risks_to_people_-_Phase_2_Guidance_Document_Technical_report.pdf). Accessed 18 July 2023
- DeKay ML, McClelland GH (1993) Predicting loss of life in cases of dam failure and flash flood. *Risk Anal* 13(2):193–205. <https://doi.org/10.1111/j.1539-6924.1993.tb01069.x>
- de Moel H, Aerts JCJH (2011) Effect of uncertainty in land use, damage models and inundation depth on flood damage estimates. *Nat Hazards* 58(1):407–425. <https://doi.org/10.1007/s11069-010-9675-6>
- de Moel H, van Alphen J, Aerts JCJH (2009) Flood maps in Europe – methods, availability and use. *Nat Hazards Earth Syst Sci* 9(2):289–301. <https://doi.org/10.5194/nhess-9-289-2009>
- de Moel H, Aerts JCJH, Koomen E (2011) Development of flood exposure in the Netherlands during the 20th and 21st century. *Glob Environ Change* 21(2):620–627. <https://doi.org/10.1016/j.gloenvcha.2010.12.005>
- de Moel H, Jongman B, Kreibich H, Merz B, Penning-Rowsell E, Ward PJ (2015) Flood risk assessments at different spatial scales. *Mitig Adapt Strateg Glob Change* 20(6):865–890. <https://doi.org/10.1007/s11027-015-9654-z>
- de Oliveira AM, Conti JB, Santos RL, de Oliveira LNA, Brito CAO, Costa FP, de Santana EN (2022) Loss of life estimation and risk level classification due to a dam break. *Heliyon* 8(4):e09257. <https://doi.org/10.1016/j.heliyon.2022.e09257>
- Di Mauro M, De Bruijn KM, Meloni M (2012) Quantitative methods for estimating flood fatalities: towards the introduction of loss-of-life estimation in the assessment of flood risk. *Nat Hazards* 63(2):1083–1113. <https://doi.org/10.1007/s11069-012-0207-4>
- Directive of the Italian Prime Minister of 8 July 2014 (2014) Indirizzi operativi inerenti all'attività di protezione civile nell'ambito dei bacini in cui siano presenti grandi dighe [Operational guidelines for civil protection activities in basins where large dams are present] (in Italian). <https://www.gazze.taufficiale.it/eli/id/2014/11/04/14A08499/sg> Accessed 18 October 2023
- D'Oria M, Maranzoni A, Mazzoleni M (2019) Probabilistic assessment of flood hazard due to levee breaches using fragility functions. *Water Resour Res* 55(11):8740–8764. <https://doi.org/10.1029/2019WR025369>
- Egorova R, van Noordwijk JM, Holterman SR (2008) Uncertainty in flood damage estimation. *Int J River Basin Manag* 6(2):139–148. <https://doi.org/10.1080/15715124.2008.9635343>
- El Bilali A, Taleb A, Boutahri I (2021) Application of HEC-RAS and HEC-LifeSim models for flood risk assessment. *J Appl Water Eng Res* 9(4):336–351. <https://doi.org/10.1080/23249676.2021.1908183>
- El Bilali A, Taleb I, Nafii A, Taleb A (2022) A practical probabilistic approach for simulating life loss in an urban area associated with a dam-break flood. *Int J Disaster Risk Reduct* 76:103011. <https://doi.org/10.1016/j.ijdr.2022.103011>
- Emilia-Romagna Region Geoportal (2021) Indicatori demografici [Demographic indicators] (in Italian). [https://servizimoka.regione.emilia-romagna.it/mokaApp/apps/DDRER\\_H5/index.html](https://servizimoka.regione.emilia-romagna.it/mokaApp/apps/DDRER_H5/index.html). Accessed 18 July 2023
- FEMA (Federal Emergency Management Agency) (2013) Federal guidelines for inundation mapping of flood risks associated with dam incidents and failures. Document FEMA P-946. FEMA, US Department of Homeland Security, Washington. [https://www.fema.gov/sites/default/files/2020-08/fema\\_dam-safety\\_inundation-mapping-flood-risks.pdf](https://www.fema.gov/sites/default/files/2020-08/fema_dam-safety_inundation-mapping-flood-risks.pdf). Accessed 18 July 2023
- FEMA (Federal Emergency Management Agency) (2021) Hazus-MH. Technical manual. FEMA, US Department of Homeland Security, Washington. [https://www.fema.gov/sites/default/files/2020-09/fema\\_hazus\\_flood-model\\_technical-manual\\_2.1.pdf](https://www.fema.gov/sites/default/files/2020-09/fema_hazus_flood-model_technical-manual_2.1.pdf). Accessed 18 July 2023
- Ferrari A, Vacondio R, Mignosa P (2023) High-resolution 2D shallow water modelling of dam failure floods for emergency action plans. *J Hydrol* 618:129192. <https://doi.org/10.1016/j.jhydrol.2023.129192>
- Fluixá-Sanmartín J, Altarejos-García L, Morales-Torres A, Escuder-Bueno I (2018) Review article: Climate change impacts on dam safety. *Nat Hazards Earth Syst Sci* 18(9):2471–2488. <https://doi.org/10.5194/nhess-18-2471-2018>
- Gazzola G (2015) L'indagine sul pendolarismo in provincia di Piacenza al XV censimento della popolazione 2011 [The survey on commuting in the province of Piacenza at the 15<sup>th</sup> population Census in 2011]. Province of Piacenza, Italy (in Italian). [https://www.piacenzaeconomia.it/Allegati/SottoLivelli/3\\_pendolarismo\\_cens2011\\_19012017-142909\\_17052019-120456.pdf](https://www.piacenzaeconomia.it/Allegati/SottoLivelli/3_pendolarismo_cens2011_19012017-142909_17052019-120456.pdf). Accessed 18 Oct 2023

- Ge W, Li Z, Liang RY, Li W, Cai Y (2017) Methodology for establishing risk criteria for dams in developing countries, case study of China. *Water Resour Manage* 31(13):4063–4074. <https://doi.org/10.1007/s11269-017-1728-0>
- Ge W, Sun H, Zhang H, Li Z, Guo X, Wang X, Qin Y, Gao W, van Gelder P (2020) Economic risk criteria for dams considering the relative level of economy and industrial economic contribution. *Sci Total Environ* 725:138139. <https://doi.org/10.1016/j.scitotenv.2020.138139>
- Ge W, Jiao Y, Wu M, Li Z, Wang T, Li W, Zhang Y, Gao W, van Gelder P (2022) Estimating loss of life caused by dam breaches based on the simulation of floods routing and evacuation potential of population at risk. *J Hydrol* 612:128059. <https://doi.org/10.1016/j.jhydrol.2022.128059>
- Graham WJ (1999) A procedure for estimating loss of life caused by dam failure. Document DSO-99-06. US Department of Interior, Bureau of Reclamation, Dam Safety Office, Denver. <https://www.usbr.gov/ssle/damsafety/TechDev/DSOTechDev/DSO-99-06.pdf>. Accessed 18 July 2023
- Hartford DND, Baecher GB (2004) Risk and uncertainty in dam safety. Thomas Telford, London
- Johnstone WM, Lence BJ (2009) Assessing the value of mitigation strategies in reducing the impacts of rapid-onset, catastrophic floods. *J Flood Risk Manag* 2(3):209–221. <https://doi.org/10.1111/j.1753-318X.2009.01035.x>
- Johnstone WM, Sakamoto D, Assaf H, Bourban S (2005) Architecture, modelling framework and validation of BC Hydro's virtual reality Life Safety Model. ISSH Stochastic Hydraulics conference, 23–24 May 2005, Nijmegen, The Netherlands
- Jonkman SN, Vrijling JK (2008) Loss of life due to floods. *J Flood Risk Manag* 1(1):43–56. <https://doi.org/10.1111/j.1753-318X.2008.00006.x>
- Jonkman SN, Vrijling JK, Vrouwenvelder ACWM (2008) Methods for the estimation of loss of life due to floods: a literature review and a proposal for a new method. *Nat Hazards* 46(3):353–389. <https://doi.org/10.1007/s11069-008-9227-5>
- Kalinina A, Spada M, Vetsch DF, Marelli S, Whealton C, Burgherr P, Sudret B (2020) Metamodeling for uncertainty quantification of a flood wave model for concrete dam breaks. *Energies* 13(14):3685. <https://doi.org/10.3390/en13143685>
- Kalinina A, Spada M, Burgherr P (2021) Quantitative assessment of uncertainties and sensitivities in the estimation of life loss due to the instantaneous break of a hypothetical dam in Switzerland. *Water* 13(23):3414. <https://doi.org/10.3390/w13233414>
- Li Z, Li W, Ge W (2018) Weight analysis of influencing factors of dam break risk consequences. *Nat Hazards Earth Syst Sci* 18(12):3355–3362. <https://doi.org/10.5194/nhess-18-3355-2018>
- Lumbroso DM, Sakamoto D, Johnstone WM, Tagg AF, Lence BJ (2011) Development of a life safety model to estimate the risk posed to people by dam failures and floods. *Dams Reserv* 21(1):31–43. <https://doi.org/10.1680/dare.2011.21.1.31>
- Lumbroso D, Davison M, Body R, Petkovek G (2021) Modelling the Brumadinho tailings dam failure, the subsequent loss of life and how it could have been reduced. *Nat Hazards Earth Syst Sci* 21(1):21–37. <https://doi.org/10.5194/nhess-21-21-2021>
- Maranzoni A, D'Oria M, Mazzoleni M (2022) Probabilistic flood hazard mapping considering multiple levee breaches. *Water Resour Res* 58(4):e2021030874. <https://doi.org/10.1029/2021WR030874>
- Maranzoni A, D'Oria M, Rizzo C (2023) Quantitative flood hazard assessment methods: a review. *J Flood Risk Manag* 16(1):e12855. <https://doi.org/10.1111/jfr3.12855>
- Masood M, Takeuchi K (2012) Assessment of flood hazard, vulnerability and risk of mid-eastern Dhaka using DEM and 1D hydrodynamic model. *Nat Hazards* 61(2):757–770. <https://doi.org/10.1007/s11069-011-0060-x>
- McClelland DM, Bowles DS (2002) Estimating life loss for dam safety risk assessment—A review and new approach. IWR Report 02-R-3. Institute for Dam Safety Risk Management, Logan, UT. <https://www.iwr.usace.army.mil/portals/70/docs/iwrreports/02-r-3.pdf>. Accessed 18 July 2023
- Merz B, Thieken AH, Gocht M (2007) Flood risk mapping at the local scale: concepts and challenges. In: Begum S, Stive MJF, Hall JW (eds) *Flood risk management in Europe*. Springer, Dordrecht, pp 231–251. [https://doi.org/10.1007/978-1-4020-4200-3\\_13](https://doi.org/10.1007/978-1-4020-4200-3_13)
- Mileti DS, Sorensen JH (2015) A guide to public alerts and warnings for dam and levee emergencies. US Army Corps of Engineers, Risk Management Center. <https://www.hsdl.org/?view&did=810121>. Accessed 9 October 2023
- Nofal OM, van de Lindt JW (2022) Understanding flood risk in the context of community resilience modeling for the built environment: research needs and trends. *Sustain Resilient Infrastruct* 7(3):171–187. <https://doi.org/10.1080/23789689.2020.1722546>
- Norkhairi FF, Thiruchelvam S, Hasini H (2018) Review methods for estimating loss of life from floods due to dam failure. *Int J Eng Technol* 7(4.35):93–97. <https://doi.org/10.14419/ijet.v7i4.35.22334>

- NZSOLD (The New Zealand Society on Large Dams) (2015) New Zealand dam safety guidelines. NZSOLD, Wellington. [https://nzsold.org.nz/wp-content/uploads/2019/10/nzsold\\_dam\\_safety\\_guidelines-may-2015-1.pdf](https://nzsold.org.nz/wp-content/uploads/2019/10/nzsold_dam_safety_guidelines-may-2015-1.pdf). Accessed 18 July 2023
- Paşa Y, Peker İB, Hacı A, Gülbaz S (2023) Dam failure analysis and flood disaster simulation under various scenarios. *Water Sci Technol* 87(5):1214–1231. <https://doi.org/10.2166/wst.2023.052>
- Penning-Rowsell E, Floyd P, Ramsbottom D, Surendran S (2005) Estimating injury and loss of life in floods: a deterministic framework. *Nat Hazards* 36(1):43–64. <https://doi.org/10.1007/s11069-004-4538-7>
- Perera D, Smakhtin V, Williams S, North T, Curry A (2021) Ageing water storage infrastructure: an emerging global risk. UNU-INWEH Report Series, Issue 11. United Nations University Institute for Water, Environment and Health, Hamilton, Canada. <https://inweh.unu.edu/wp-content/uploads/2021/01/Ageing-Water-Storage-Infrastructure-An-Emerging-Global-Risk.pdf>. Accessed 18 Oct 2023
- Pilotti M, Maranzoni A, Tomirotti M, Valerio G (2011) 1923 Gleno dam break: case study and numerical modeling. *J Hydraul Eng* 137(4):480–492. [https://doi.org/10.1061/\(ASCE\)HY.1943-7900.0000327](https://doi.org/10.1061/(ASCE)HY.1943-7900.0000327)
- Poortvliet PM, Knotters M, Bergsma P, Verstoep J, van Wijk J (2019) On the communication of statistical information about uncertainty in flood risk management. *Saf Sci* 118:194–204. <https://doi.org/10.1016/j.ssci.2019.05.024>
- Qi H, Altınakar MS (2012) GIS-based decision support system for dam break flood management under uncertainty with two-dimensional numerical simulations. *J Water Resour Plan Manag* 138(4):334–341. [https://doi.org/10.1061/\(ASCE\)WR.1943-5452.0000192](https://doi.org/10.1061/(ASCE)WR.1943-5452.0000192)
- RESCDAM (2001) Loss of life caused by dam failure, the RESCDAM LOL method and its application to Kyrkösjärvi dam in Seinäjoki. [https://civil-protection-humanitarian-aid.ec.europa.eu/system/files/2014-11/rescdam\\_rapportfin.pdf](https://civil-protection-humanitarian-aid.ec.europa.eu/system/files/2014-11/rescdam_rapportfin.pdf). Accessed 18 July 2023
- Resolution of the Regional Council of Emilia-Romagna no. 967 of 14 May 2018 (2018) Piano di emergenza – Diga di Mignano [Emergency plan of the Mignano dam] (in Italian). <https://protezionecivile.regione.emilia-romagna.it/gestione-emergenze/piani-emergenza-dighe-ped/diga-di-mignano>. Accessed 4 July 2023
- Rizzo C, Maranzoni A, D’Oria M (2023) Probabilistic mapping and sensitivity assessment of dam-break flood hazard. *Hydrol Sci J* 68(5):700–718. <https://doi.org/10.1080/02626667.2023.2174026>
- Rodrigues AS, Santos MA, Santos AD, Rocha F (2002) Dam-break flood emergency management system. *Water Resour Manage* 16(6):489–503. <https://doi.org/10.1023/A:1022225108547>
- Sarchani S, Koutroulis AG (2022) Probabilistic dam breach flood modeling: the case of Valsamiotis dam in Crete. *Nat Hazards* 114(2):1763–1814. <https://doi.org/10.1007/s11069-022-05446-0>
- Saxena KR, Sharma VM (2004) Dams: incidents and accidents. CRC Press, Boca Raton, FL
- Silva AFR, Eleutério JC (2023a) Analysis of flood warning and evacuation efficiency by comparing damage and life-loss estimates with real consequences related to the São Francisco tailings dam failure in Brazil. *Nat Hazards Earth Syst Sci* 23(9):3095–3110. <https://doi.org/10.5194/nhess-23-3095-2023>
- Silva AFR, Eleutério JC (2023b) Effectiveness of a dam-breach flood alert in mitigating life losses: a spatiotemporal sectorisation analysis in a high-density urban area in Brazil. *Water* 15(19):3433. <https://doi.org/10.3390/w15193433>
- Sun R, Wang X, Zhou Z, Ao X, Sun X, Song M (2014) Study of the comprehensive risk analysis of dam-break flooding based on the numerical simulation of flood routing. Part I: model development. *Nat Hazards* 73(3):1547–1568. <https://doi.org/10.1007/s11069-014-1154-z>
- Teng J, Jakeman AJ, Vaze J, Croke BFW, Dutta D, Kim S (2017) Flood inundation modelling: a review of methods, recent advances and uncertainty analysis. *Environ Model Softw* 90:201–216. <https://doi.org/10.1016/j.envsoft.2017.01.006>
- Tsai CW, Yeh JJ, Huang CH (2019) Development of probabilistic inundation mapping for dam failure induced floods. *Stoch Environ Res Risk Assess* 33(1):91–110. <https://doi.org/10.1007/s00477-018-1636-8>
- Vacondio R, Dal Palù A, Ferrari A, Mignosa P, Aureli F, Dazzi S (2017) A non-uniform efficient grid type for GPU-parallel Shallow Water equations models. *Environ Model Softw* 88:119–137. <https://doi.org/10.1016/j.envsoft.2016.11.012>
- Vorogushyn S, Merz B, Lindenschmidt KE, Apel H (2010) A new methodology for flood hazard assessment considering dike breaches. *Water Resour Res* 46(8):W08541. <https://doi.org/10.1029/2009WR008475>
- Wagenaar DJ, De Bruijn KM, Bouwer LM, De Moel H (2016) Uncertainty in flood damage estimates and its potential effect on investment decisions. *Nat Hazards Earth Syst Sci* 16(1):1–14. <https://doi.org/10.5194/nhess-16-1-2016>
- Yerramilli S (2013) Potential impact of climate changes on the inundation risk levels in a dam break scenario. *ISPRS Int J Geo-Inf* 2(1):110–134. <https://doi.org/10.3390/ijgi2010110>
- Zhang L, Peng M, Chang D, Xu Y (2016) Dam failure mechanisms and risk assessment. Wiley, Singapore

---

**Publisher's Note** Springer Nature remains neutral with regard to jurisdictional claims in published maps and institutional affiliations.